Stable Ti_n ($n = 2-15$) Clusters and Their Geometries: DFT Calculations

Martin Salazar-Villanueva,[†] Pedro H. Hernández Tejeda,[†] Umapada Pal,[†] Jose F. Rivas-Silva,[†] Jose I. Rodríguez Mora,[†] and Jorge A. Ascencio*[,‡]

Instituto de Física, Universidad Autónoma de Puebla, Apdo. Postal J-48, Puebla, Pue. 72570, Mexico and Instituto Mexicano del Petróleo, Lázaro Cárdenas 152, Col San Bartolo Atepehuacan, México Distrito Federal, C.P. 07730, México

Received: March 2, 2006; In Final Form: June 30, 2006

We present a detailed structural analysis for small Ti_n ($n = 2-15$) clusters based on ab initio quantum mechanical calculations of their binding energies, frontier orbital gaps, and second energy derivatives. Local density approximation calculations revealed that while the smaller clusters ($n \leq 8$) prefer hexagonal atomic arrays with bulklike crystal symmetry, the bigger clusters prefer pentagonal atomic arrays. From the stability criteria of the magic number clusters we could identify three magic number clusters Ti_7, Ti_{13}, and Ti_{15}. While the most stable configuration of Ti_7 is a decahedral bipyramid induced by tetrahedral atomic arrays, the most stable configuration of Ti_{13} is an icosahedron. The other stable cluster Ti_{15} takes a closed-shell icosahedron-like configuration with both pentagonal and hexagonal symmetries. The stability of the Ti_n clusters strongly depends on their geometries and charge states. The HOMO−LUMO gap of the Ti_n clusters approaches its bulk value for $n > 8$. While there is not much difference between the HOMO and LUMO isosurface charge distributions for the Ti_7 and Ti_{13} clusters in their most stable configurations, they are very different in the case of Ti_{15}. Such a distinct charge distribution in Ti_{15} indicates its singular chemical selectivity over the other two magic number clusters.

1. Introduction

With the vast application prospects of metallic nanoparticles, understanding the atomic aggregation process, configuration, and stability, in particular, has become an important goal for experimental and theoretical research.[1−4] The task, without doubt, is very important for understanding nanotechnology principles and applications, especially for material selection and their designing.[1,2] In particular, the nonmetallic−metallic transition behavior of metallic clusters has been of great scientific and technological interest during the past two decades,[5,6] and study of the size evolution of atomic aggregates from clusters toward bulk is of great importance. While use of sophisticated instruments such as scanning tunneling microscopy (STM) and scanning tunneling spectroscopy (STS) made the task easier for experimentalists, use of classical molecular[3] and quantum mechanical approaches[4] with the help of new codes and computational capabilities became obligatory for theoretical studies.

According to the electronic configuration of titanium ([Ar] $3d^2 3s^2$), it has an open-shell d orbital with only two electrons. Its lowest energy configuration and corresponding electronic properties have attracted attention in several investigations.[7−9] Formation of its magic number clusters and their geometries are a matter of discussion among theoreticians and experimentalists. Most agree that those clusters have a pentagonal preferential arrangement. Wu et al.[8] have shown that for clusters bigger than $n = 8$, the 3d states hardly influence the growth of 5-fold structures. Such a preference in structural form is due to the tendency of the atoms to align as repeated tetrahedral units, searching for the most stable spherical geometries,[10] as it has been identified through high-resolution electron microscopy (HREM) for Au,[11,12] Pd,[13] Pt,[14] and other metallic clusters including bimetallic[15−18] ones. It is well known that the bulk structure corresponds to a minimum energy array, and consequently, many metallic clusters tend to find atomistic distributions with geometries similar to the bulk unit cells for certain number of atoms,[2,12] which for Ti would correspond to structures based on hexagons and decahedra.

Experimental STS studies on metallic clusters have shown that for clusters less than 1 nm in size, the difference between the highest occupied molecular orbital (HOMO) and lowest unoccupied molecular orbital (LUMO) increases with a decrease in cluster size up to a few atoms.[9]

The magic number clusters are highly stable as they have closed-shell geometries, high binding energy per atom, large ionization potential, and wide band gaps. Such characteristics of the magic number clusters have been extensively probed for Nb, with closed-shell configurations for Nb_8, Nb_{10}, and Nb_{16}.[19] However, the cluster charges can influence their electronic and atomic configurations as has been observed for Al_n[20] and Cu_n[21] clusters among others.

To study the nonmetallic−metallic transition in Ti_n clusters, we calculated the lowest energy configurations for $n = 2-15$ along with their corresponding stable structures to understand their stability and electronic properties. It is seen that the band gap depends strongly on the cluster charge, and the Ti_7, Ti_{13}, and Ti_{15} clusters acquire closed-shell configurations. These magic number Ti_n clusters are in good agreement with the predictions of Sakurai et al.[22] through their time-of-flight (TOF) measurements. Using molecular simulations based on density

* To whom correspondence should be addressed. Phone: +52 55 91758461. Fax: +52 55 91756429. E-mail: ascencio@imp.mx. http://www.paginasprodigy.com/jascenciogtz/.
[†] Universidad Autónoma de Puebla.
[‡] Instituto Mexicano del Petróleo.

10.1021/jp061332e CCC: $33.50
Published on Web 08/03/2006

TABLE 1: Equilibrium Bond Length r_0 and Binding Energy E_b for Ti_2 Cluster in Comparison with Other Reported Values

	calcd[a]	exp[b]	calcd[c]	calcd[d]	calcd[e]
r_0 (au)	3.660	3.677	3.720	3.580	3.721
E_b (eV)	3.883	1.540	0.320	4.724	3.857

[a] Report with tight-binding approximation.[29] [b] Experimental data.[30] [c] Report with Hartree−Fock approximation.[31] [d] Present calculation with LDA. [e] Present calculation with GGA.

functional theory (DFT) with a local density approximation, the binding energy, second energy derivatives, HOMO, and LUMO for the clusters are analyzed.

2. Computational Method

Geometry optimization and electronic property calculations were performed using DMol3 software[23,24] (as a module of Cerius2 by Accelrys), which is a first-principle method and allows working with no periodic structures. DMol3 uses the real space framework within DFT.[25] This code allows the study of small structures giving information about interatomic distance, angles, and torsion for the lowest energy configurations. We used the generalized gradient approximation (GGA) with the functional parametrization proposed by Lee et al.[26] Geometry optimizations were performed considering an energy change per atom of 1×10^{-5} Hartree, a force media square of 0.002 Hartree/Å, and allowed displacement square of 0.005 Å/atom. All calculations are carried out without spin restriction (this allows establishing the lowest energy geometries and maximum of convergence and considering a norm-conserving pseudopotential[27] for optimizations. Only the spins for the lowest energy configurations were determined. The maxima of the binding energy (E_b) are defined as $E_b = E_i - E_t$, where E_i is the sum of the energies of individual atoms and E_t is the total energy of the system. The second energy derivative could be expressed as $\Delta E(n) = E(n+1) + E(n-1) - 2E(n)$, where $E(n)$ is the binding energy of the cluster with n atoms. The electronic gaps were evaluated for the lowest energy structures with positive, negative, and neutral charges from their corresponding energy differences between the HOMO and LUMO.

3. Results and Discussion

3.1. *Ti_n* Clusters and Their Geometries. To evaluate the accuracy of our calculations, parameters such as bond length, r_0, and binding energy, E_b, used in the present work were initially compared with the results for a two-atom array for which plenty of theoretical and experimental results are available. The values of the parameters obtained though our LDA and GGA calculations are presented in Table 1 along with other reported values. We can see that our bond length and binding energy values obtained for the Ti_2 cluster are in good agreement with the previously reported values, though our E_b value is a bit overestimated. Besides, we calculated the oscillation frequency of this dimer to be 404.4 cm^{-1}, which is in good agreement with the experimental value (407.9 cm^{-1}) obtained by Cossé et al.[28]

It is well known that in bulk form titanium has a compact hexagonal crystalline structure. Therefore, in 2-D planer array clusters, the dominance of hexagonal base with a central atom in their lowest energy configuration (as shown in Figure 1a) is not surprising. While for Ti_4 the preferential structure is a rhombus, with an energy difference of 0.2892 eV with respect to its square geometry, for Ti_7 the planer configuration is composed of three rhombuses. A similar trend can be seen also for Ti_{10} and Ti_{12} clusters, where the clusters naturally tend to form flat structures with rhombic geometries.

To obtain minimum energy structures, a large number of possible geometries were considered. The structures were optimized and the lowest energy configurations obtained as shown in Figure 1b. The clusters with a tetrahedral array of atoms show a similar tendency to those of other metallic clusters forming octahedral, decahedral, etc., up to icosahedral isomers for 13 atoms. However, very interesting lowest energy configurations are observed for the Ti_8 and Ti_{15} clusters, where the isomers acquire hexagonal geometries, characteristic of Ti bulk. The parallel and antiparallel arrays of rhombuses in the configurations of Ti_8 and Ti_{15} are evidence of the large influence of bulk symmetry on the larger clusters. In clusters of lowest energy configurations, such a characteristic transition is not common for other elements. Ti_{15}, in particular, is a kind of polyhedron, quite similar to an icosahedron but based in hexagonal and pentagonal symmetries, which requires a large amount of energy to be generated from the decahedral clusters. This structure corresponds to 24 isoscale triangles: two groups of six triangles in the top and bottom hexagonal pyramids which are in antiparallel alignment and 12 more isoscale triangles produced by their coupling. On the other hand, Ti_{16}, Ti_{17}, and Ti_{18} clusters are not highly stable because of their binding energy and electronic gap values as can be seen in Figures 2 and 3. However, these clusters tend to acquire the shape associated to the next magic number cluster of titanium, the Ti_{19} one.[22] The symmetry, binding energy, and bond length of the most representative clusters we calculated are presented in Table 2, which are in good agreement with the reported results of Wei et al.[29] In fact, for smaller clusters the binding energy values of their isomers with varying geometries are very close, and they can coexist in a real synthesis process.

3.2. Cluster Stability and Nonmetallic−Metallic Transition. To compare our results with the reported results of magic number clusters (Ti_n, $n = 7$ and 13), the criteria of localizing the maxima in the binding energy and second energy derivative curves defined by Zhao et al.[32] and Castro et al.[33] were taken into account. Because of the relevance of the spin for these clusters, the influence of the spin state on their lowest energy configurations was established. In fact, considering the spin in our calculations, we determined the binding energy and equilibrium bond length values to be very similar to the values obtained without spin restriction (see Supporting Information).

An interesting feature of the Ti_3 cluster is that a slightly distorted equilateral triangular geometry is favored with $\Delta E = 0.0245$ eV over the isoscale triangular structure. As the energy difference between these geometries is small, both structures can coexist at low temperature. Similarly for Ti_4 cluster, the configuration of a regular tetrahedron with a distortion of 0.8% in one of the points (and a spin multiplicity of 5) is favored with an energy difference $\Delta E = 0.027$ eV over an equilateral triangular configuration with an in-plane central atom. While the most stable geometry found for Ti_5 is a distorted triangular bipyramid (C_{2v}), with an energy difference of 0.287 eV over the square-based pyramid geometry (D_{3h}), the most stable structure of Ti_6 is an octahedron with O_h symmetry. The most stable Ti_7 cluster possess D_{5h} symmetry with $\Delta E = 0.133$ eV from the nearest most stable configuration based on a square array. A detailed stability analysis of the clusters revealed that the Ti_7 cluster is a magic number cluster with well-defined peaks in the binding energy and second energy derivative curves (Figure 2). For Ti_8 clusters, a three-dimensional rhombus with D_{6h} symmetry is most favorable, which has an energy difference

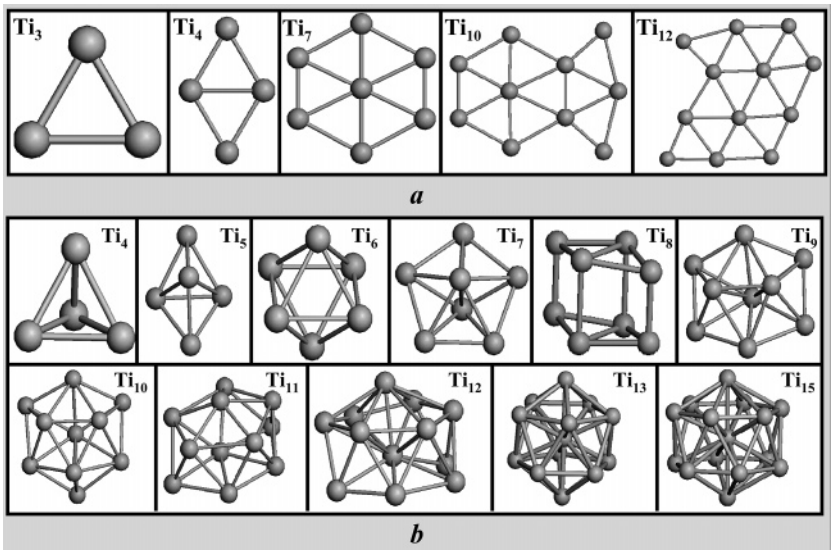

Figure 1. Lowest energy configurations of Ti_n for (a) two-dimensional arrays ($n = 4, 7, 10, 12$) and (b) three-dimensional clusters ($n = 4-13, 15$).

TABLE 2: Binding Energy Per Atom E_b and Average Bond Length r_0 for the Most Stable Ti_n ($n = 2-15$) Clusters with Their Corresponding Symmetries[a]

n	symmetry	E_b (eV)	r_0 (au)	M	n	symmetry	E_b (eV)	r_0 (au)	M
2	linear	**1.929**	**1.969**		9	C_{2v}	**3.381**	**2.682**	
3	D_{3h}	**2.229**	**2.418**		9	C_{2v}	3.370	2.632	1
3	D_{3h}	2.219	2.375	5	9	D_{7h}	3.286	2.635	
3	C_{2v}	2.205	2.213		9	D_{2h}	3.146	2.596	
3	linear	2.308	2.188		10	C_{3v}	**3.440**	**2.669**	
4	T_d	**2.643**	**2.488**	5	10	C_{3v}	3.433	2.659	1
4	T_d	2.641	2.445		10	D_{4h}	3.221	2.633	
4	D_{2h}	2.616	2.352		10	C_{2v}	3.140	2.602	
4	D_{4h}	2.592	2.289		11	C_{2v}	**3.493**	**2.668**	
5	C_2	**2.944**	**2.569**		11	C_{2v}	3.490	2.631	1
5	C_{2v}	2.892	3.267	3	11	C_s	3.621	2.642	
5	D_{3h}	2.657	2.492		11	D_{4h}	3.436	2.632	
5	D_{4h}	2.133	2.412		12	C_s	**3.512**	**2.713**	1
6	O_h	**3.075**	**2.636**		12	D_{5h}	3.511	2.693	
6	O_h	3.028	2.625		12	C_s	3.338	2.642	
6	D_{4h}	2.942	2.591		12	C_{2v}	3.081	2.624	
6	C_{5v}	2.952	2.563		13	I_h	**3.669**	**2.701**	
7	D_{5h}	**3.286**	**2.625**	1	13	I_h	3.669	2.693	1
7	D_{5h}	3.265	2.575		13	C_{2v}	3.473	2.969	
7	C_{2v}	3.246	2.603		13	D_{3h}	3.370	2.923	
7	D_{2h}	3.209	2.594		14	C_{2v}	**3.688**	**2.747**	1
8	C_s	**3.255**	**2.626**		14	O_h	3.687	2.705	
8	C_s	3.233	2.620	3	15	D_{6d}	**3.772**	**2.805**	1
8	D_{6h}	3.243	2.597		15	D_{6d}	3.771	2.712	
8	D_{3h}	3.004	2.580		15	C_{6v}	3.679	2.639	

[a] The most stable geometries are marked in bold. M = spin multiplicity.

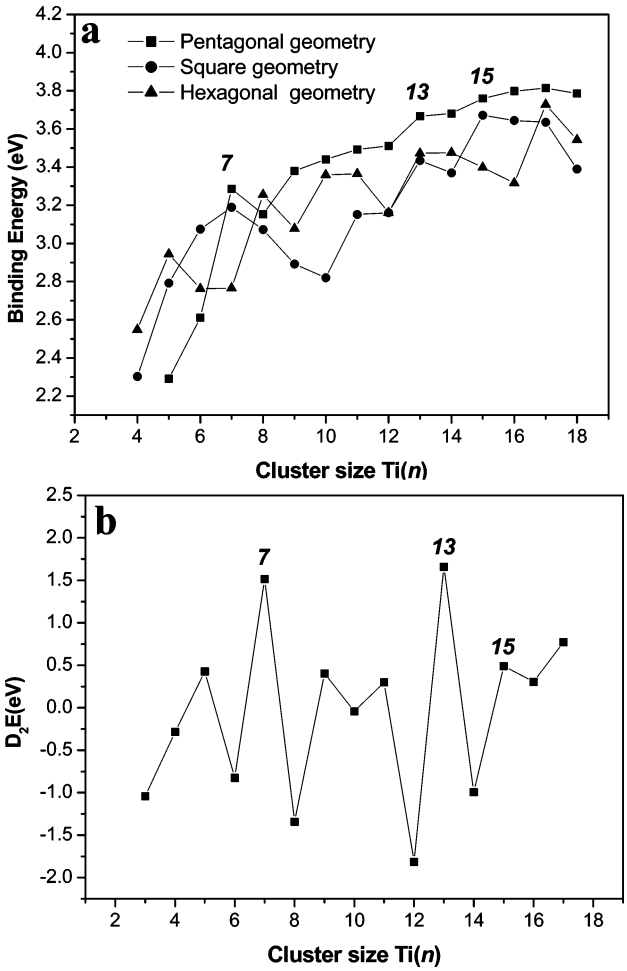

Figure 2. Stability plots for the Ti clusters: (a) binding energy variation with cluster size for the most stable square, hexagonal, and pentagonal geometries and (b) second energy difference variation with cluster size for clusters with pentagonal geometries. The local maxima in the curves denote high stability of the cluster.

of 0.0129 eV with respect to the truncated pentagonal bipyramid geometry with C_s symmetry. The stable rhombus-like geometry shows a clear influence of bulk array in bigger Ti_n clusters. Similar stable geometries are seen for Ti_n, $n = 9-12$, where the rhombus-based geometries convert to recursive pentagonal pyramids on adding extra atoms and finally convert to icosahedron for Ti_{13}. This most stable icosahedron geometry of Ti_{13} has energy differences of 0.169, 0.196, and 0.299 eV with respect to its decahedral, hexagonal, and *fcc* structures, respectively, as observed by Wang et al.[34] For Ti_{15} an icosahedral-like structure with 24 triangular faces is the most stable geometry. Interestingly, the antiparallel hexagonal configuration in Ti_{15} with a spin multiplicity of 1 leads to pentagonal arrays of atoms. Such a configuration has $\Delta E = 0.094$ eV over the decahedral configuration, which is the next stable geometry for this cluster. We must notice that the Ti_9 cluster with a truncated icosahedron geometry passes through a structural transition on

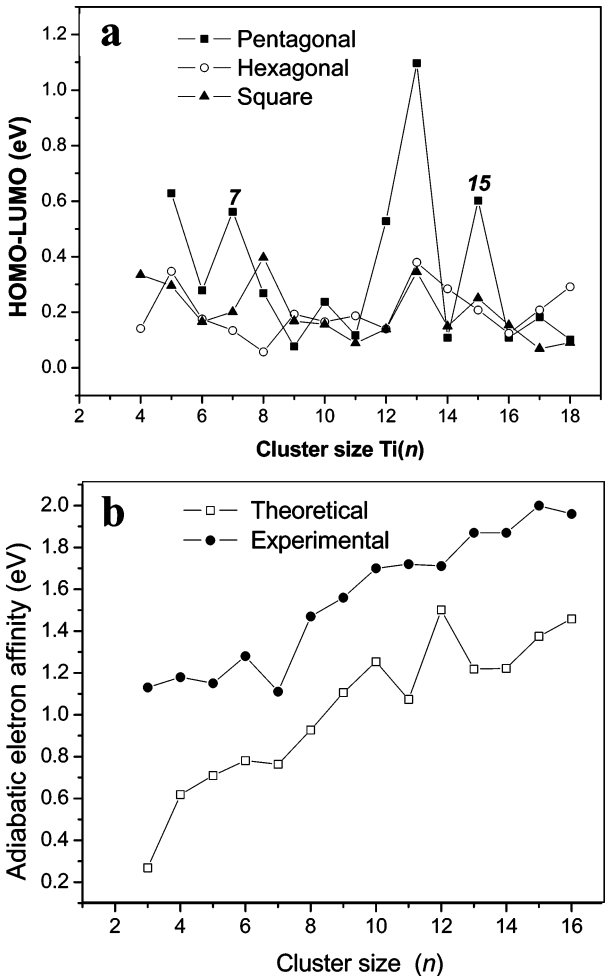

Figure 3. Variation of HOMO−LUMO gap with cluster size for (a) the most stable neutral Ti_n clusters with square, hexagonal, and pentagonal geometries and (b) the most stable Ti_n clusters with pentagonal symmetries with different charges.

addition of extra atoms to reach a more stable Ti_{13} magic number cluster. On addition of further atoms in the cluster, another highly stable cluster T_{15} with a closed-shell geometry similar to that of Ti_7 and Ti_{13} magic number clusters was obtained. In the binding energy and second energy derivative curves presented in Figure 2, we see sharp maxima for $n = 7$, 13, and 15. Though the Ti_{15} cluster basically possesses hexagonal symmetry, careful observation reveals a mixture of pentagonal and hexagonal arrays in it. The spherical shape in the form of the icosahedral-like geometry of the Ti_{15} cluster generated through combination of 6-fold and 5-fold symmetries resulting is highly stable. Incorporating the spin state in binding energy calculations we observed that it has no significant influence on reaching the lowest energy configurations for smaller clusters, as reported previously.[33] However, for the clusters of nine or more atoms, consideration of the spin state $M = 1$ (see Table 2) allows reaching the most stable configurations, which must be associated with the characteristic open-shell $4s^23d^2$ or $4s^13d^3$ of Ti atoms.

Using binding energy plots for clusters of different sizes and geometries we can extract information about the aggregation tendency of the atoms to produce lowest energy configurations. Stability plots for the Ti_n clusters with different geometries are shown in Figure 2. We can see that while for very small clusters a hexagonal geometry is favorable, for clusters bigger than Ti_8 a pentagonal geometry is favored over hexagonal and square geometries.

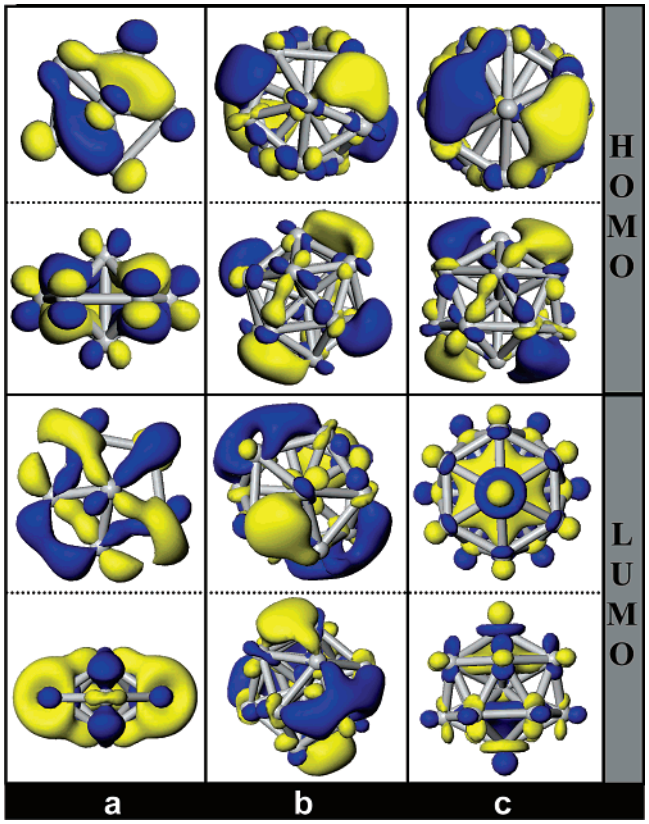

Figure 4. Analysis of HOMO and LUMO isosurfaces for (a) Ti_7, (b) Ti_{13}, and (c) Ti_{15} clusters with top (upper ones) and side (lower ones) views.

To study the nonmetallic−metallic transition in Ti_n clusters and their stability further we calculated their HOMO and LUMO energies. The HOMO−LUMO gaps for clusters with different geometries are plotted in Figure 3a. While the smaller clusters revealed semiconductor-like behavior, a metallic bulk-like characteristic was revealed for bigger clusters, in agreement with the observations of Wang et al.[34] While most of the clusters with $n > 8$ show metallic behavior with HOMO−LUMO gaps close to the bulk value, the Ti_{13} and Ti_{15} clusters with pentagonal closed-shell geometries fulfill the stability conditions of magic number cluster[35] with high HOMO−LUMO gaps. It must be noticed that for Ti aggregates with $n < 8$ the charge distribution is mainly through participation of p and d orbital electrons and the contribution of s electrons is insignificant. For $n \geq 8$, the density of i and p electrons increases significantly, decreasing the density of d electrons, generating a process known as a metallic transition as is evident from their energy gap values. This tendency can also be observed in the electron affinity plots (Figure 3b), which are very similar to the experimentally observed variations,[36] for most of the clusters.

In Figure 4 the HOMO and LUMO charge distributions generated from the geometrical atomistic array of Ti_7, Ti_{13}, and Ti_{15} magic number clusters are presented. While the Ti_{15} cluster revealed preferential sites for the HOMO and homogeneous charge distribution for the LUMO, there are no significant differences between the HOMO and LUMO for the Ti_7 and Ti_{13} clusters. Such a distinct charge distribution characteristic of the Ti_{15} cluster implies its better chemical selectivity over the other two magic number clusters.

Our detailed analysis identified not only the magic number Ti_7, Ti_{13}, and Ti_{15} clusters, but also their other interesting properties not studied earlier. It must be mentioned that though a hexagonal configuration has been identified for the sodium

magic number clusters,[35] most of the other metallic magic number clusters correspond to icosahedral configurations with two extra atoms around. The high symmetry of the Ti_{15} cluster implies a clear difference in its electronic structure with respect to smaller magic number clusters (Ti_7 and Ti_{13}). The high stability of the Ti_{15} structure suggests the possibility of formation of bigger clusters with similar symmetry, like Ti_{46}, Ti_{65}, Ti_{175}, Ti_{369}, Ti_{671}, Ti_{1105}, Ti_{1695}, and Ti_{2465} (see, for instance, additional information for $n = 175$) through shell-by-shell growth, following the magic number clusters with mixed icosahedral and fcc-like structures (Ti_{38}, Ti_{55}, Ti_{147}, Ti_{309}, Ti_{561}, Ti_{923}, Ti_{1415}, Ti_{2057}, etc.). The corresponding increase of atoms in the clusters is based on the shell-to-shell growth, as established by the golden rule of Fibonacci.[37] Besides, the hexagonal tendency of Ti metal in bulk must be favorable for formation of these structural configurations. Apart from determination of the geometries of fcc-like, icosahedral, and decahedral structures which have been well studied and characterized, an exhaustive search must be made for identification of these low-energy configurations using simulated patterns. Simulated images of a Ti_{175} cluster with their corresponding model and electron diffraction pattern (calculated by using SimulaTEM,[38] which is based on the multislice method and image formation theory for TEM[39]) at its different orientations can be seen in the Supporting Information.

4. Conclusions

Through DFT calculations we determined the most stable geometries and corresponding binding energies of Ti_n clusters for $n = 2-18$. For small clusters of nonmetallic character ($n < 8$), spin consideration affects the structural and electronic properties, while the effect of spin is much less for bigger clusters. For flat structures the most stable cluster configurations are generated through the hexagonal distribution of atoms in two-dimensional space similar to bulk titanium. Among the three-dimensional clusters, closed-shell configurations of Ti_7, Ti_{13}, and Ti_{15} in neutral charge state have greater stability.

Our calculations revealed the most stable magic number clusters of Ti_7 and Ti_{13} with pentagonal atomic arrays of bipyramidal decahedral and icosahedral shape, respectively, as reported earlier. However, we identified Ti_{15} as a magic number cluster with an interesting geometrical configuration, which is basically 24 triangular faces in array of six and five and highly spherical having a central atom and 14 atoms in the vertexes. While the difference between the HOMO and LUMO isosurface charge distributions for the Ti_7 and Ti_{13} magic number clusters is small, the situation is quite different in the case of the Ti_{15} cluster, indicating its better chemical selectivity over the former.

While for bigger clusters ($n > 8$) a pentagonal geometry is clearly favored energetically, for smaller clusters ($n < 8$) they can coexist in pentagonal, hexagonal, or square arrays. In general, clusters with $n > 8$ have metallic behavior. Except for magic number clusters, the difference between the HOMO and LUMO is relatively small, especially for the bigger clusters, and they can coexist in experimental synthesis processes. The chemical reactivity of the clusters depends strongly on their charge conditions. These physicochemical properties show a high dependence on the spin state for clusters smaller than $n = 8$.

Acknowledgment. M.S.V. thanks Lucero Ballinas R. for useful discussions and suggestions. This work was partiality supported by CONACYT (México) by means of scholarship No.183758.

Supporting Information Available: Direct comparison of energy plots for optimized geometries with restricted and unrestricted spin; structures, simulated HREM images, and electron diffraction patterns of the Ti_{175} cluster useful for recognizing this type of cluster experimentally. This material is available free of charge via the Internet at http://pubs.acs.org.

References and Notes

(1) Freeman, D. L.; Doll, J. D. *Annu. Rev. Phys. Chem.* **1996**, *47*, 43.

(2) Jose-Yacaman, M.; Ascencio, J. A.; Liu, H. B. *J. Vac. Sci. Technol., B* **2001**, *19*, 1091.

(3) Liu, H. B.; Perez, R.; Canizal, G.; Ascencio, J. A. *Surf. Sci.* **2002**, *518*, 14.

(4) Wedensky, D. D. *J. Phys.: Condens. Matter* **2004**, *16*, R1537.

(5) Berkowitz, A. E. In *Magnetic Properties of Fine Particles*; Dormann, J. L., Fioriani, J. L., Eds.; North-Holland: Amsterdam, 1992.

(6) Alonso, J. A. *Chem. Rev.* **2000**, *100*, 637.

(7) Wang, S. Y.; Duan, W.; Zhao, D. L.; Wang, C. Y. *Phys. Rev. B* **2002**, *65*, 165424.

(8) Wu, H.; Desai, S. R.; Wang, L. S. *Phys. Rev. Lett.* **1996**, *76*, 212.

(9) Vinod, C. P.; Kulkarni, G. U.; Rao, C. N. R. *Chem. Phys. Lett.* **1998**, *289*, 329.

(10) Ascencio, J. A.; Pérez, M.; Jose-Yacaman, M. *Surf. Sci.* **2000**, *447*, 73.

(11) Ascencio, J. A.; Perez, M.; Tehuacanero, S.; Jose-Yacaman, M. *Appl. Phys. A* **2001**, *73*, 295.

(12) Ascencio, J. A.; Gutierrez-Wing, C.; Espinosa-Pesqueira, M. E.; Tehuacanero, S.; Zorrilla, C.; Jose-Yacaman, M. *Surf. Sci.* **1998**, *396*, 349.

(13) Jose-Yacaman, M.; Marin, M.; Ascencio, J. A. *J. Mol. Catal. A* **2001**, *3154*, 1.

(14) Jose-Yacaman, M.; Ascencio, J. A.; Tehuacanero, S.; Marin, M. *Top. Catal.* **2002**, *18*, 167.

(15) Pal, U.; Sanchez-Ramírez, J. F.; Liu, H. B.; Medina, A.; Ascencio, J. A. *Appl. Phys. A* **2004**, *79*, 79.

(16) Ely, T. O.; Pan, C.; Amiens, C.; Chaudret, B.; Dassenoy, F.; Lecante, P.; Casanove, M. J.; Mosset, A.; Respaud, M.; Broto, J. M.; *J. Phys. Chem. B* **2000**, *104*, 695.

(17) Ascencio, J. A.; Mejia, Y.; Liu, H. B.; Angeles, C.; Canizal, G. *Langmuir* **2003**, *19*, 5882.

(18) Moskovits, M.; Srnova-Sloufova, I.; Vlckova, B. *J. Chem. Phys.* **2002**, *116*, 10435.

(19) Kietzmann, H.; Morenzin, J.; Bechtlod, P. S.; Gantefor, G.; Eberhardt, W. *J. Chem. Phys.* **1998**, *109*, 2275.

(20) Rao, B. K.; Jena, P. *J. Chem. Phys.* **1999**, *111*, 1890.

(21) Calaminici, P.; Koster, A. M.; Russo, N.; Salahub, D. R. *J. Chem. Phys.* **1996**, *105*, 9546.

(22) Sakurai, M.; Watanabe, K.; Sumiyama K.; Suzuki, K. *J. Chem. Phys.* **1999**, *111*, 235.

(23) Delley, B. *J. Chem. Phys.* **1990**, *92*, 508.

(24) Delley, B. *J. Chem. Phys*. **1991**, *94*, 7245.

(25) Hohenberg, P.; Kohn, W. *Phys. Rev. B* **1964**, *136*, 864.

(26) Lee, C.; Yang, W.; Parr, R. G. *Phys. Rev. B* **1988**, *37*, 786.

(27) Hamann, D. R.; Schluter, M.; Chiang, C. *Phys. Rev. Lett.* **1979**, *43*, 20.

(28) Cossé, C.; Fouassier, M.; Mejean, T.; Traquile, M.; DiLella, D. P.; Moskovists, M. *J. Chem. Phys.* **1980**, *73*, 6076.

(29) Wei, S. H.; Zhi, Z.; You, J. Q.; Yan, X. H.; Gong, X. G. *J. Chem. Phys.* **2000**, *113*, 11127.

(30) Russon, L. M.; Heldecke, S. A.; Birke, M. K.; Conceicao, J.; Morse, M. D.; Armentrout, P. B. *J. Chem. Phys.* **1994**, *100*, 4747.

(31) Morse, M. D. *Chem. Rev.* **1986**, *86*, 1049.

(32) Zhao, J.; Qiu, Q.; Wang, B.; Wang, J.; Wang, G. *Solid State Commun.* **2001**, *118*, 157.

(33) Castro, M.; Liu, S. R.; Zhai, H. J.; Wang, L. S. *J. Chem. Phys.* **2003**, *118*, 2116.

(34) Wang, S. Y.; Yu, J.; Mizuseki, Z. H.; Yan, J. A.; Kawazoe, Y. *J. Chem. Phys.* **2004**, *120*, 18.

(35) Sattler, K. In *Handbook of Thin Films Materials*; Naiwa, H. S., Ed.; Academia Press: Los Angeles, 2002; Vol. 5, Chapter II, p 17.

(36) Liu, S. R.; Zhai, H. J.; Castro, M.; Wang, L. S. *J. Chem. Phys.* **2003**, *118*, 2108.

(37) Macia, E. *Rep. Prog. Phys.*, **2006**, *69*, 397.

(38) Gomez, A.; Beltran, L. *SimulaTEM Software*; Unam, Mexico, 2000; http://www.fisica.unam.mx.

(39) Ascencio, J. A.; Castaño, V. M. *Optik* **1998**, *108*, 83.